J Appl Electrochem (2010) 40:955–965
DOI 10.1007/s10800-009-9815-4

ORIGINAL PAPER

Developments in the soluble lead-acid flow battery

R. G. A. Wills · J. Collins · D. Stratton-Campbell · C. T. J. Low · D. Pletcher · Frank C. Walsh

Received: 29 October 2008 / Accepted: 26 January 2009 / Published online: 1 March 2009

Abstract The history of soluble lead flow batteries is concisely reviewed and recent developments are highlighted. The development of a practical, undivided cell is considered. An in-house, monopolar unit cell (geometrical electrode area 100 cm^2) and an FM01-LC bipolar (2×64 cm^2) flow cell are used. Porous, three-dimensional, reticulated vitreous carbon (RVC) and planar, carbon-HDPE composite electrodes have been used in laboratory flow cells. The performance of such cells under constant current density (10–160 mA cm^{-2}) cycling is examined using a controlled flow rate (mean linear flow velocity <14 cm s^{-1}) at a temperature of approximately 298 K. Voltage versus time and voltage versus current density relationships are considered. High charge (<90%), voltage (<80%) and energy (<70%) efficiencies are possible. Possible failure modes encountered during early scale-up from a small, laboratory flow cell to larger, pilot-scale cells are discussed.

For special issue of Journal of Applied Electrochemistry (Ed., K. Bouzek), 8th European Electrochemical Engineering Symposium, 26 January 2009.

R. G. A. Wills · C. T. J. Low · F. C. Walsh (✉)
Energy Technology Research Group, School of Engineering Sciences, University of Southampton, Southampton SO17 1BJ, UK
e-mail: f.c.walsh@soton.ac.uk

J. Collins · D. Stratton-Campbell
C-Tech Innovation Ltd., Capenhurst, Chester CH1 6EH, UK

D. Pletcher
Electrochemistry and Surface Science Group, School of Chemistry, University of Southampton, SO17 1BJ Southampton, UK

Keywords Bipolar flow batteries · Lead · Lead dioxide · Methanesulfonic acid · Porous · Three-dimensional electrodes

1 Introduction

Energy storage systems are becoming increasingly important as an essential component in power efficiency and distribution systems. Large-scale energy storage devices will be required for full and effective integration of renewable sources (e.g., wind and solar-systems) into the current production/distribution networks. Redox flow batteries have been proposed as one solution to energy storage and load levelling problems. A number of redox couples have been proposed for use within large-scale flow batteries. Operational technologies include bromine/polysulfide, all vanadium, zinc/bromine and zinc/cerium [1]. The soluble lead-acid flow battery is in the early stages of development but has a significant advantage over other systems in its ability to operate with a single electrolyte without the need for a cell-dividing membrane.

Traditional lead-acid batteries (e.g., SLI, starting lighting ignition) batteries for automotive applications) operate with an electrolyte, typically sulphuric acid, in which lead compounds are only sparingly soluble. Consequently, an insoluble paste containing the active materials is normally applied to each of the electrodes. Lead-acid batteries containing lead in the solution phase (or whose reaction products are soluble) have been suggested but not widely produced. Table 1 provides a chronological profile of the progression towards a soluble lead redox flow cell.

A number of batteries using perchloric, fluorosilicic, or fluoroboric acid electrolytes that have soluble lead salt discharge products have been described [2–5]. These are all

Table 1 A concise literature summary that outlines developments in soluble lead-acid flow batteries

Year	Type	Configuration	Listed electrolytes	Reference
1946	Primary	Box cell	$HClO_4/HBF_4/H_2SiF_6$	[2]
1947	Primary	Box cell	$HClO_4$	[3]
1949	Primary	Box cell/circulated electrolyte	$HClO_4$	[4]
1972	Primary	Box cell	HBF_4	[5]
1977	Secondary	Box cell	$HClO_4/HBF_4/H_2SiF_6/H_3NO_3S$	[6]
1978	Secondary	Box cell/flow cell	$HBF_4/H_2SiF_6/H_3NO_3S$	[7]
1982	Secondary	Button cell	H_2SiF_6/CH_3SO_3H	[8]
2004	Secondary	Undivided bipolar flow cell	CH_3SO_3H	[9]
2004	Secondary	Undivided bipolar flow cell	CH_3SO_3H	[10]
2005	Secondary	Undivided bipolar flow cell	CH_3SO_3H	[11]
2005	Secondary	Undivided bipolar flow cell	CH_3SO_3H	[12]
2008	Secondary	Undivided monopolar flow cell	CH_3SO_3H	[13, 14]
2006	Secondary	Divided bipolar flow stack	$R–SO_3H/R–PO_3H_2$ R = alkyl group, e.g., $–CH_3$	[15]

primary batteries, however, and are predominantly designed as dry reserve batteries where the acid is introduced into the cell immediately before use. Their electrodes are produced via electrochemical plating or pasting of active material onto the current collectors. These batteries can produce a high current density for a short period of time and are often targeted to small-scale emergency operations; such devices usually return relatively low-voltage efficiency.

Several patents [6–8] have described secondary batteries with electrolytes containing soluble lead. These tend to be small box/button cells with electrolytes typically comprising perchloric acid, hexafluorosilicic acid or fluoroboric acid. Henk et al. [8] made use of lead methanesulfonate as an additive to the predominantly lead silicofluoride electrolyte, while Wurmb et al. [7] circulated the electrolyte within the battery, using separate redox couples (e.g., Fe^{2+}/Fe^{3+}) as additives to enhance the performance.

A series of papers by Pletcher et al. [9–12] has described the electrochemistry and performance of a small (typically 2 cm^2 geometric electrode area) laboratory flow cell based on an electrolyte containing solvated lead(II) ions in aqueous methanesulfonic acid. The electrode and cell reactions are well established, at the positive electrode:

$$PbO_2 + 4H^+ + 2e^- \underset{\text{Charge}}{\overset{\text{Discharge}}{\rightleftarrows}} Pb^{2+} + 2H_2O \quad (1)$$

at the negative electrode:

$$Pb \underset{\text{Charge}}{\overset{\text{Discharge}}{\rightleftarrows}} Pb^{2+} + 2e^- \quad (2)$$

resulting in an overall cell reaction:

$$Pb + PbO_2 + 4H^+ \underset{\text{Charge}}{\overset{\text{Discharge}}{\rightleftarrows}} 2Pb^{2+} + 2H_2O \quad (3)$$

During charge, lead is deposited at the negative electrode while lead dioxide deposits at the positive one. During discharge, the lead and lead dioxide layers redissolve via oxidation and reduction, respectively, back to the soluble lead(II) ion. Electrochemical measurements have shown that both the Pb/Pb^{2+} and Pb^{2+}/PbO_2 redox couples are suitable for use with a methanesulfonic acid electrolyte and substantial lead and lead dioxide layers could be reversibly deposited and stripped from a number of electrode materials [9–12]. The kinetics of the Pb^{2+}/PbO_2 couple were noticeably slower than those of the Pb/Pb^{2+} couple and some inefficiency was introduced due to the lead dioxide electrode. The dendritic nature of electrodeposited lead layers also requires careful consideration. Additives that enhance the quality of the lead deposit morphology, increase the kinetics of the lead dioxide electrode, and reduce shedding of PbO_2 have been investigated [12]. Recent papers have described the effects of electrolyte composition (including additives) and operating conditions on the performance of the lead [13] and lead dioxide [14] electrodes in soluble lead-acid flow cells, in some detail.

A recent patent [15] describes a redox flow battery operating with similar chemistry but all of the examples include cell division by a separator and few process details are given.

This paper describes the development and scale-up of the soluble lead redox flow battery and is the first account to show this battery system operating on a significant scale. An ICI FM01-LC flow reactor was used, firstly in single cell and secondly in two-cell, bipolar configurations, before the system was further developed using a custom-built flow cell. The charge/discharge characteristics for these batteries

are discussed along with some of the failure modes encountered during the scale-up process.

2 Experimental details

2.1 General

The preparation of solutions has been described previously [9]. Unless otherwise stated, the initial electrolyte comprised lead methanesulfonate (1.5 mol dm^{-3}) and ligninsulfonic acid (1.0 g dm^{-3}) in aqueous methanesulfonic acid (1.0 mol dm^{-3}) at approximately 298 K.

2.2 Cells

Two cells were used in early scale-up studies of the soluble lead-acid flow battery. Table 2 summarizes the characteristics of these cells and compares them with the 2 cm^2 cell used in previous work [10].

2.2.1 64 cm^2 electrode cell

A flow cell was constructed from an ICI FM01-LC laboratory reactor [16–18], using stainless-steel plates for the current collectors and end plates. The electrode materials were reticulated vitreous carbon [17, 18] (RVC), carbon felt, or nickel foam. The electrodes were aligned so that the flow of electrolyte was lengthwise and the geometric area of each electrode was 4 cm wide × 16 cm long. The RVC foam was 1 or 13 mm thick, the carbon felt was 8 mm thick, and the nickel foam was 1 mm thick. The electrodes were secured to the current collectors using Leit-C conductive carbon cement, which also served to protect the steel from corrosion. A number of bipolar electrodes were trialled. In all cases, the electrode material was either RVC or Ni foam. The support for the RVC of Ni foams was made from stainless steel, carbon, or a PTFE gasket. In each case, conductive carbon cement was used to attach the RVC/Ni foams to the support. For the PTFE gasket, the carbon cement also formed a barrier between cells preventing leakage currents. An inter-electrode gap of 4 mm was established using elastomeric gaskets, which also formed the flow channel. The cell was operated either as a two-electrode, parallel plate reactor or as a four-electrode, two-cell, bipolar stack. Figure 1 shows the bipolar arrangement.

2.2.2 100-cm^2 electrode cell

A custom-made flow cell was designed and built in collaboration with C-Tech Innovation Limited. It operated with electrodes having geometric surface areas of 100 cm^2 (10 × 10 cm^2). The cell was constructed so that the inter-electrode spacer frame could also contain spiral flow channels incorporated into the inlet and outlet manifolds. This would increase the inter-cell flow path for scaling up to a bipolar system. Between the spiral channels and the main, 10 × 10 cm, cell cavity, removable plenum chambers were placed, acting as flow distributors. The inter-electrode gap was 10 mm. Copper plates were used as current collectors. This flow cell was fitted with planar carbon-HDPE composite electrodes [10] and contained an

Table 2 Comparison of three experimental cells used during the early laboratory development and scale-up of the soluble lead flow battery

Property	Previous 2 cm^2 cell	64 cm^2 cell	100 cm^2 cell
Positive electrode material	3-D RVC	3-D RVC or carbon felt	Planar C-HDPE composite
Negative electrode materials	3-D RVC or Ni foam	3-D RVC or Ni foam[a]	Planar C-HDPE composite
Number of positive electrodes	1	1 (monopolar mode) or 2 (bipolar mode)	1
Geometrical area of each electrode/cm^2	2	64	100
Total area of positive electrodes/cm^2	2	64 or 128	100
Initial inter-electrode gap/cm	0.40–1.6	0.40	0.15–1.5
Volumetric flow rate of electrolyte/ cm^3 min^{-1}	4.0	4.0–14	4.0–20
Mean linear flow velocity of electrolyte/ cm s^{-1}	2–10	2–10	2–15
Current collector material	Carbon-polymer composite plate	316 Stainless-steel plate	Copper plate
Electrolyte volume in reservoir/cm^3	40–100	250	500

RVC Reticulated vitreous carbon (90 ppi), *C-HDPE* Carbon-high density polyethylene

[a] 90 ppi nickel foam

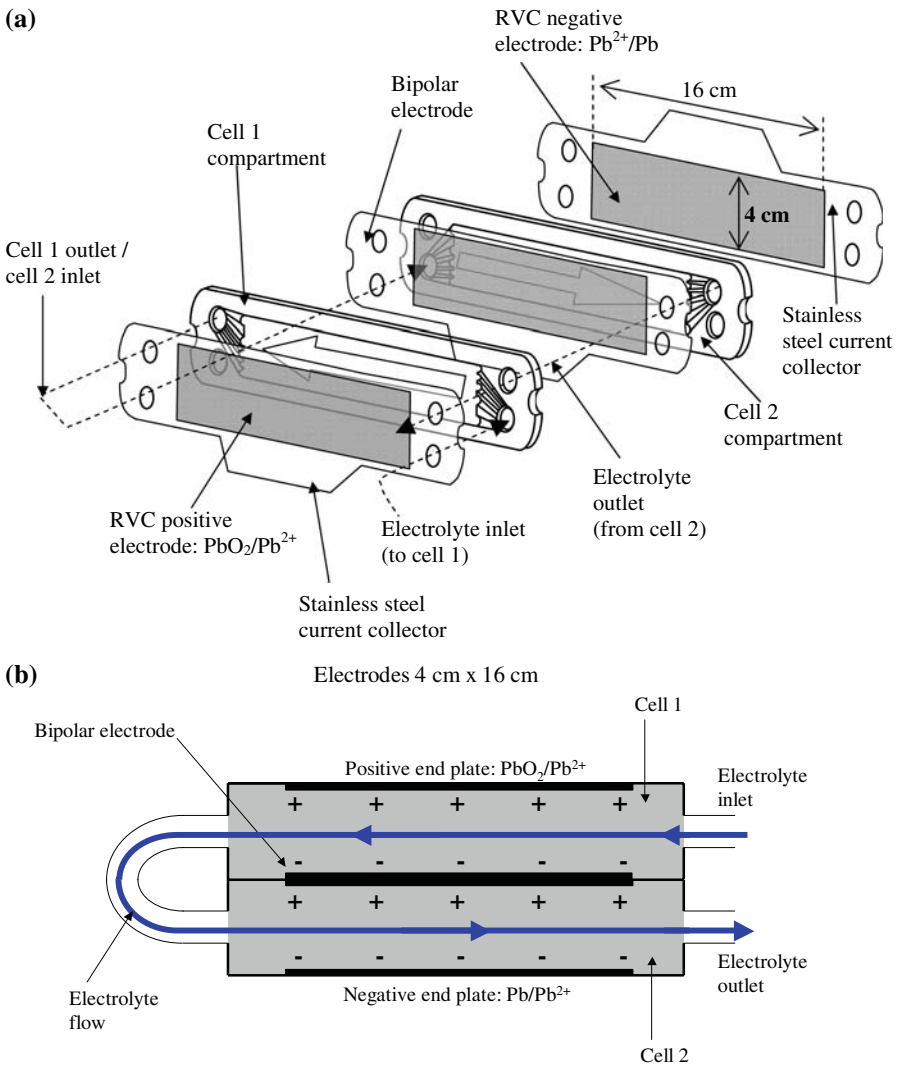

Fig. 1 Schematic representation of **a** the FM-01-LC bipolar stack and **b** diagram of the bipolar flow system

extended flow path between cells to reduce the bypass currents which could result in dendritic lead and lead-dioxide growths. The cell was operated using three flow chamber configurations, as shown in Fig. 2. (A) The spacer frame (including inlet manifold and plenum chamber) was replaced by a rubber gasket giving a 'V'-shaped electrolyte inlet path. (B) The second configuration utilized the spacer frame, inlet manifold, and plenum chamber. (C) The third configuration utilized the spacer frame, inlet manifold, and plenum chamber fitted with mesh to provide a turbulent electrolyte flow.

2.3 Procedures

Charging currents were applied using a Thurlby Thandar Instruments model TSX1820P DC laboratory power supply. Electronic loads were drawn from the battery using a Thurlby Thandar Instruments LD300 DC electronic load.

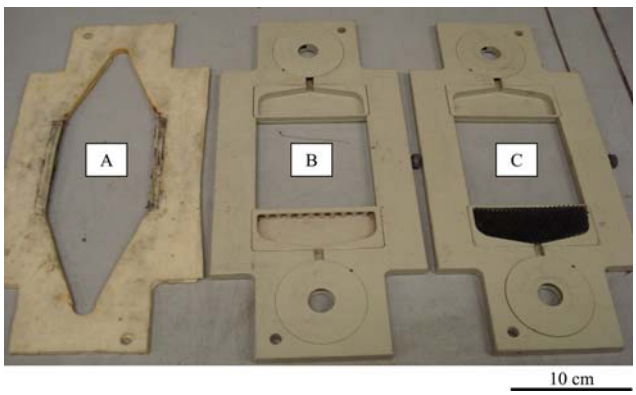

Fig. 2 Photographic images showing the three flow chamber configurations used in the larger, 100 cm^2 cell. (A) Silicone gasket forming the flow chamber. (B) Flow chamber comprising the spacer frame, inlet manifold, and plenum chamber. (C) Flow chamber comprising spacer frame, inlet manifold, and plenum chamber fitted with mesh to provide turbulent electrolyte flow

Cell voltages/potentials were measured using a National Instruments NI USB-9215A portable USB data acquisition device coupled to a PC running National Instruments' NI-DAQmx and VI Logger Lite acquisition software. Current densities are quoted using the geometric footprint of the electrode material at the current collector plates.

Experiments were performed at ambient temperature (298 ± 2 K). The volumetric flow rate of the electrolyte through the cell was between 4 and 14 $cm^3\ s^{-1}$ and the electrolyte reservoir volume was varied between 250 and 1,000 cm^3.

3 Further flow cell developments

3.1 ICI FM01-LC cell

The ICI FM01-LC flow cell was designed as a general-purpose electrochemical reactor; in the present studies, it was adapted to demonstrate the soluble lead RFB operating in the bipolar mode. A number of electrode configurations were tested as summarized in Table 3, where the number of completed cycles is given along with the associated efficiencies and failure mode. The time periods and current densities during charge/discharge cycles were varied; the total charge/total discharge values are given to show the total of all cycles for each experiment.

A two-cell electrode stack was assembled from the FM01-LC cell, using RVC (dimensions: 16.0 × 4.0 × 0.1 cm^3) for both the positive and negative electrodes. The battery was charged for 3 h at 20 mA cm^{-2}. The stack was dismantled, following charging, to inspect the electrode deposits. Lead and lead dioxide deposits were visible on both sets of electrodes (Fig. 3). The deposited material was evenly distributed over each of the electrode surfaces and throughout the RVC foam structure. No dendrites or noticeable edge effects were observed on the lead layers. This indicated that, with the chosen cell configuration and under the operating conditions used, satisfactory current and electrolyte flow distribution was achieved.

The two-cell bipolar stack was reassembled with fresh electrodes. The positive electrode material was RVC foam (16 × 4 × 1.3 cm, 90 ppi), the negative electrode material was nickel foam (16 × 4 × 0.1 cm, 90 ppi) and the current collectors/electrode supports were stainless-steel plates (ca. 2 mm thick). Following a number of charging and discharging periods to condition the battery, a series of charge-discharge cycles was performed. The cycles consisted of a 15-min charge followed by a 15-min discharge, using a current density of 20 mA cm^{-2} throughout. The voltage response to charging and load currents was comparable to the smaller cell used in previous studies [10]. The voltage-versus-time plot is shown in Fig. 4. The combined stack voltage for the two cells was approximately 3.7 V during charge and 3.4 V during discharge. The voltage of each individual cells was approximately 1.8 V during charge and 1.7 V during discharge. Within a multi-cell battery stack it is important that the performance of each cell be comparable. Any disparity between cells would eventually lead to state-of-charge differences and stack failure. As can be seen in Fig. 4 the voltages of the two cells were identical, indicating comparable active material utilization in each cell.

After further conditioning, the cell was subjected to a series of 1-min charge and 1-min discharge cycles. The current density was incremented by 20 mA cm^{-2} for each

Table 3 FM-01-LC cell configurations and charge/discharge operation data. Electrolyte: 1.5 mol dm^{-3} Pb^{2+} and 1 g dm^{-3} ligninsulfonic acid in 1.0 mol dm^{-3} CH_3SO_3H

Cells	Electrodes	Number of cycles	Total charge (A h)	Total discharge (A h)	Charge efficiency (%)	Voltage efficiency (%)	Failure mode
2	1-mm-thick RVC	10	7.5	4.8	64	88	Pb dendrites
2	13-mm-thick RVC (+ve), 1-mm-thick Ni foam (−ve)	11	9.0	5.4	61	91	Pb dendrites and/or PbO_2 sludge
1	1-mm-thick RVC (+ve), 1-mm-thick Ni foam (−ve)	19	16.4	8.8	54	81	PbO_2 sludge
2	Monopoles: 1-mm-thick RVC bipole: 1-mm-thick RVC on PTFE support	8	4.5	1.8	40	78	Failure of bipolar electrode
2	Monopoles: 1-mm-thick RVC bipole: 1-mm-thick RVC on Toray carbon support	12	8.5	5.4	64	86	Failure of bipolar electrode
1	1-mm-thick RVC	25	26.2	11.6	44	78	PbO_2 sludge
1	8-mm-thick carbon felt (+ve) 1-mm-thick RVC (−ve)	14	12.2	6.3	52	70	PbO_2 sludge

Electrolyte mean linear flow velocity: 4–20 cm s^{-1}. Current density 10–100 mA cm^{-2}. All RVC material was approximately 90 ppi grade

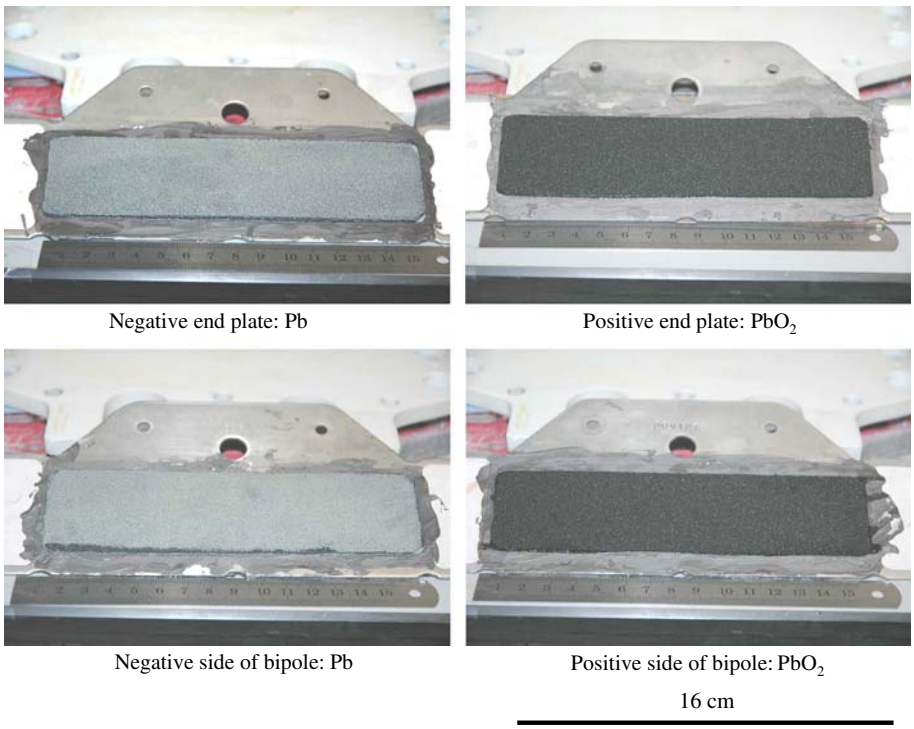

Fig. 3 Photographic images showing electrodeposits after a 3-h charge, in the 64 cm^2 electrode cell, at 20 mA cm^{-2}

subsequent cycle and the battery voltage was recorded. The voltage versus current density plots for charging and discharging are given in Figs. 5 and 6, respectively. The voltage obtained at various current densities is determined by a number of factors, including *IR* drop across the electrolyte channel and the electrodes, the kinetics of the two electrode reactions, and mass transport of the lead(II) to and from the electrode surfaces. The charging voltage increased linearly with applied current density, which suggested that the cell/stack resistance (approximately 0.63 Ω) was the dominating factor. The electrolyte had a relatively high conductivity [9] such that ohmic drop between the electrodes should be small with a 5-mm-thick flow channel. During discharge there was a non-linear drop in cell voltage for increasing current densities, indicating that the stack conductivity was less important. During

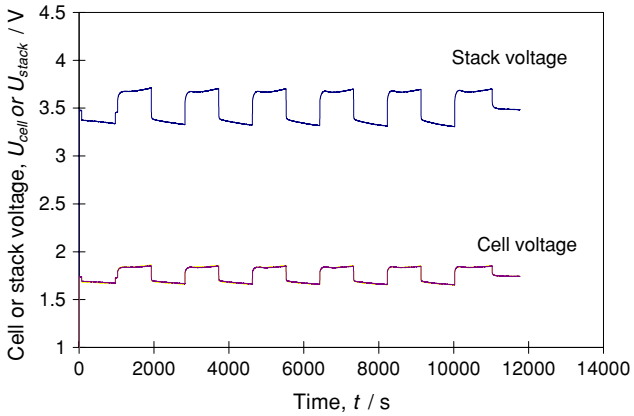

Fig. 4 Cell voltage versus time profile for repeated charging and discharging of the flow battery. A current density of 20 mA cm^{-2} was used throughout. The positive electrode was 1.3-cm-thick RVC (90 ppi) and the negative electrode was 1-mm-thick Ni foam (90 ppi). The inter-electrode spacing was 5 mm. The reservoir was filled with 500 mL of electrolyte which was pumped through the battery with a volumetric flow rate of 15 cm^3 s^{-1} (corresponding to a mean linear flow velocity of 3 cm s^{-1})

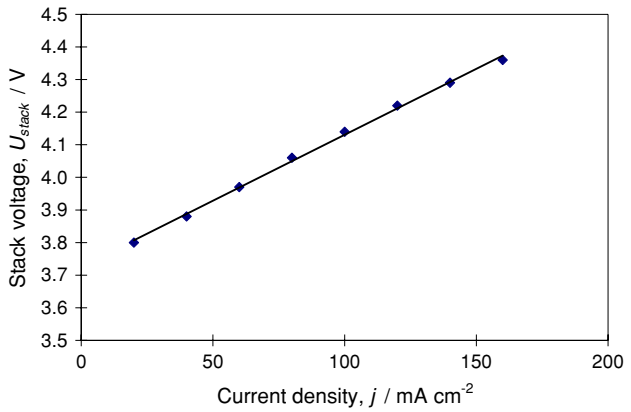

Fig. 5 Cell voltage versus current density data for the 64 cm^2 electrode battery on charge. Cell voltage values were obtained after 1 min at a controlled current density in the range 20–160 mA cm^{-2}. The positive electrode was 1.3-cm-thick RVC (90 ppi) and the negative electrode was 1-mm-thick Ni foam (90 ppi). The inter-electrode spacing was 5 mm. The reservoir was filled with 500 mL of electrolyte, which was pumped through the battery at a volumetric flow rate of 15 cm^3 s^{-1} (3 cm s^{-1})

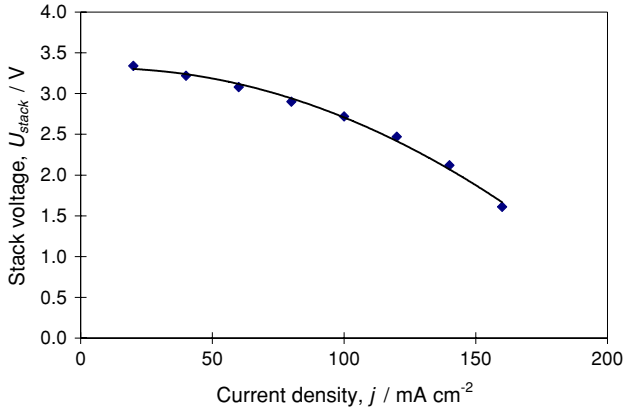

Fig. 6 Cell voltage versus current density data for the 64-cm^2 electrode battery on discharge. Cell voltage values were obtained after 1 min at a controlled current density. The positive electrode was 1.3-cm-thick RVC (90 ppi) and the negative electrode was 1-mm-thick Ni foam (90 ppi). The inter-electrode spacing was 5 mm. The reservoir was filled with 500 mL of electrolyte, which was pumped through the battery with a volumetric flow rate of 15 cm^3 s^{-1} (3 cm s^{-1})

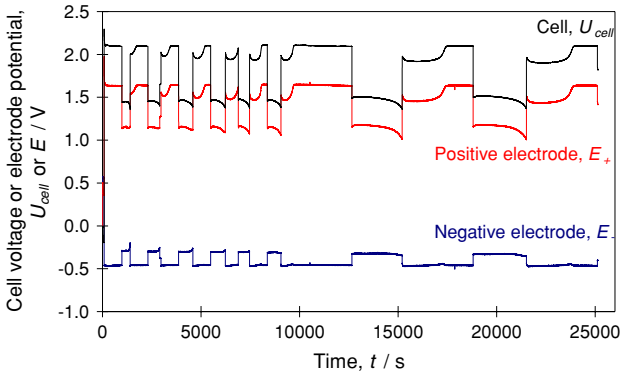

Fig. 7 Cell voltage versus time profile for the 100 cm^2 flow cell. The reservoir was filled with 1,000 mL of electrolyte, which contained 1 g dm^{-3} ligninsulfonic acid and was pumped through the battery at a volumetric flow rate of 15 cm^3 s^{-1}. The inter-electrode spacing was 6 mm, with a mean linear flow velocity of 2.5 cm s^{-1}

discharge it is likely that a combination of the kinetics for lead dioxide reduction and mass transport of reaction products away from the electrode surface had a dominant affect on the cell voltage. The data demonstrated operation of a bipolar soluble lead-acid flow battery on a scale which is 32 times the geometric area of the 2-cm^2 electrodes used in early studies [10].

3.2 100-cm^2 in-house flow cell

A 100-cm^2 cell was custom-built in collaboration with C-Tech Innovation Limited and was designed specifically for the soluble lead-acid battery. Table 4 summarizes the experimental data obtained with this cell. Specific details of successful cycling results are given below.

The large cell was fitted with two carbon composite electrodes, each with geometric surface area of 100 cm^2. The true surface area of the electrodes was increased by impregnating the surface with crushed RVC fragments. The electrolyte initially comprised Pb^{2+} (1.5 mol dm^{-3}), CH_3SO_3H (1.0 mol dm^{-3}), and ligninsulfonic acid (1 g dm^{-3}). The inter-electrode spacing was 1.5 cm and the mean linear flow velocity was 14 cm s^{-1}. The electrolyte reservoir, which was maintained at 298 K, contained 0.5 dm^3 of electrolyte. A series of constant current (20 mA cm^{-2}) charge and discharge cycles were used. Each cycle consisted of a set charge followed by a discharge until the voltage dropped to 1.2 V. In total, six 15-min charges, 23 60-min charges, and one 250-min charge with associated discharges were carried out. Figure 7 presents the voltage-versus-time profile for the six short (14 or 15 min) cycles and the first three 1-h charge cycles. The plot shows the overall cell voltage along with the voltage of the positive and negative electrodes, measured versus an SCE reference electrode. This series of charge/discharge cycles shows that the flow battery may be successfully operated for an extended period. During the later, 1-h cycles, dendritic electrode formations began to short-circuit the cell. Despite this, the charge efficiency remained consistently above 60%. Over longer-term

Table 4 100-cm^2 cell configuration and operational data

Electrodes	Flow configuration	Number of cycles	Total charge (A h)	Total discharge (A h)	Charge efficiency (%)	Voltage efficiency (%)	Failure mode
Carbon polymer composite with RVC granules	C	35	65.7	38.0	58	72	Pb dendrites and PbO_2 sludge
Carbon polymer composite with RVC granules	A	126	49.0	33.0	67	77	Pb dendrites
Carbon polymer composite with RVC granules	A	30	30.7	16.9	55	76	Creep of PbO_2 deposit
Carbon polymer (Entegris)	B	11	3.0	2.6	87	73	Creep of PbO_2 deposit

Electrolyte: 1.5 mol dm^{-3} Pb^{2+} and 1 g dm^{-3} ligninsulfonic acid in 1.0 mol dm^{-3} CH_3SO_3H. Mean linear flow velocity of electrolyte: 4–20 cm s^{-1}. Current density: 10–100 mA cm^{-2}

operation such electrode deposits must be avoided by the use of suitable electrolyte additives and appropriate operational parameters.

The cell was fitted with fresh electrodes, which comprised of a planar carbon composite plate (without 3-D RVC particles) having a surface area of 100 cm^2. A series of 100 charge/discharge cycles (constant current of 10 mA cm^{-2}) was applied using an electrolyte initially comprising Pb^{2+} (1.5 mol dm^{-3}) in aqueous CH_3SO_3H (1.0 mol dm^{-3}). No electrolyte additives were used. The electrolyte (0.5 dm^{-3}) was maintained at 298 K in a thermostated reservoir. Table 5 summarizes the data obtained. Following the initial few cycles, the cell performance became predictable and consistent. Charge, voltage, and energy efficiencies were approximately 90, 80, and 70%, respectively. Furthermore, no shorting or irregular electrode deposit morphology was observed.

Figure 8 shows a series of charges using incremented current densities. Between each charge period the cell was left on open-circuit and the cell voltage was monitored. Following the incremental charges, an analogous set of discharges were performed. During open-circuit periods between charges, the open-circuit voltage decayed slowly towards a steady value; between the discharge periods, the open-circuit voltage rapidly reached a steady value. Figure 8 also shows that the slow decay in voltage observed in rest periods between charging is almost entirely associated with the positive electrode. During cell operation, the pH of the electrolyte will vary and this variation may be much greater with the thick PbO_2 layers at the positive electrode, as indicated in reaction (1). During PbO_2 deposition, it is likely that the surface is significantly more acidic than the bulk electrolyte, particularly if small quantities of electrolyte are trapped within the growing deposit. The pH gradient generated would take time to equilibrate with the bulk electrolyte and may account for the open-circuit voltage drop. According to the Nernst equation for the soluble lead system, the open-circuit voltage is expected to increase at a higher pH [11].

Table 5 Efficiency data for the 100 cm^2 geometric electrode area flow cell fitted with planar C-HDPE composite electrodes

Cycle number	Charge efficiency (%)	Voltage efficiency (%)	Energy efficiency (%)
1	68	77	52
5	73	78	57
10	87	79	69
20	90	79	71
40	90	80	72
60	88	81	71
80	87	81	71
100	91	81	74

The initial electrolyte was 1.5 mol dm^{-3} Pb^{2+} in 1.0 mol dm^{-3} CH_3SO_3H. The electrolyte reservoir (0.5 dm^3) was maintained at 298 K. Inter-electrode gap = 10 mm. Volumetric flow rate of electrolyte = 14 cm^3 s^{-1}. Constant current density during charge and discharge = 10 mA cm^{-2}. Charge time = 15 min

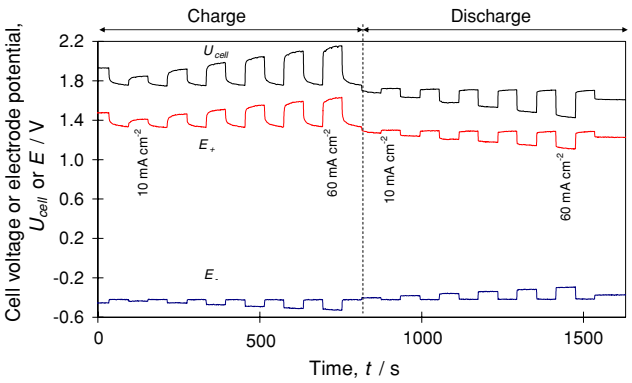

Fig. 8 Cell-voltage-versus-time profile for the 100-cm^2 flow cell showing the effect of current density on the charge and discharge voltages. The reservoir was filled with 1,000 mL of electrolyte, which contained 1 g dm^{-3} ligninsulfonic acid and was pumped through the battery at a volumetric flow rate of 15 cm^3 s^{-1}. The inter-electrode spacing was 6 mm, giving a mean linear flow velocity of 2.5 cm s^{-1}

Operation of the 100-cm^2 cell demonstrates the soluble lead chemistry on a 50-fold increased scale compared to previous (2-cm^2) work [10–12]. The ratio between the cell channel circumference and the geometric area of a 100-cm^2 electrode is 0.4 cm^{-1}. The same ratio for a 2-cm^2 electrode is 3 cm^{-1}. Edge effects define the characteristics such as mass transport and current distribution, of smaller electrodes to a greater degree than for larger electrodes. Operation of the soluble lead-acid battery on 100-cm^2

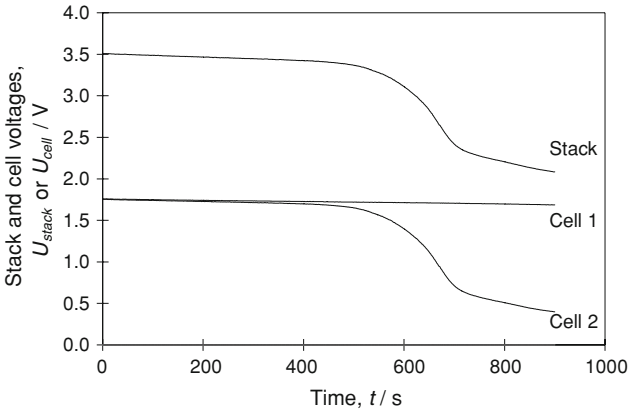

Fig. 9 Cell voltage-versus-time data for a failing bipolar battery stack. A current density of 20 mA cm^{-2} was used throughout the discharge. The positive electrode was 1.3-cm-thick RVC (90 ppi) and the negative electrode was 1-mm-thick Ni foam (90 ppi). The inter-electrode spacing was 5 mm. The reservoir was filled with 500 mL of electrolyte that was pumped through the battery at a volumetric flow rate of 15 cm^3 s^{-1} (mean linear flow velocity of 2.5 cm s^{-1})

electrodes demonstrates that lead and lead-dioxide layers can be deposited on, and stripped off, electrodes having larger geometric areas. This is encouraging for future scale-up leading to commercially viable energy storage systems based on the soluble lead-acid battery technology.

3.3 Battery failure analysis

Operating over short charge periods (<1 A h) the battery was capable of a relatively long life (>100 cycles) and a high efficiency (ca. 90% charge efficiency). However, with the formation of thicker electrode deposits over >2 A h charge periods) cycle life decreased significantly.

Bipolar battery failure may be attributed to compromised structural integrity of the cell (e.g., cracking of the bipolar electrode) or imbalances of cell chemistry. As mentioned above, any efficiency differences between cells in a bipolar stack will impair the battery performance. If structural failure of a bipolar electrode occurs, two or more cells will be compromised. Figure 9 shows the discharge curve for a two-cell battery that was in the process of failing due to imbalances in the cell chemistry. At the beginning of the discharge period, a steady 3.5 V was maintained by the battery, with both cells operating at 1.75 V. After approximately 500 s, the battery voltage drops off sharply. The loss of performance was entirely due to the second cell, with the cell one continuing to maintain a reasonably high stack voltage. Three problems associated with the cell chemistry have been identified;

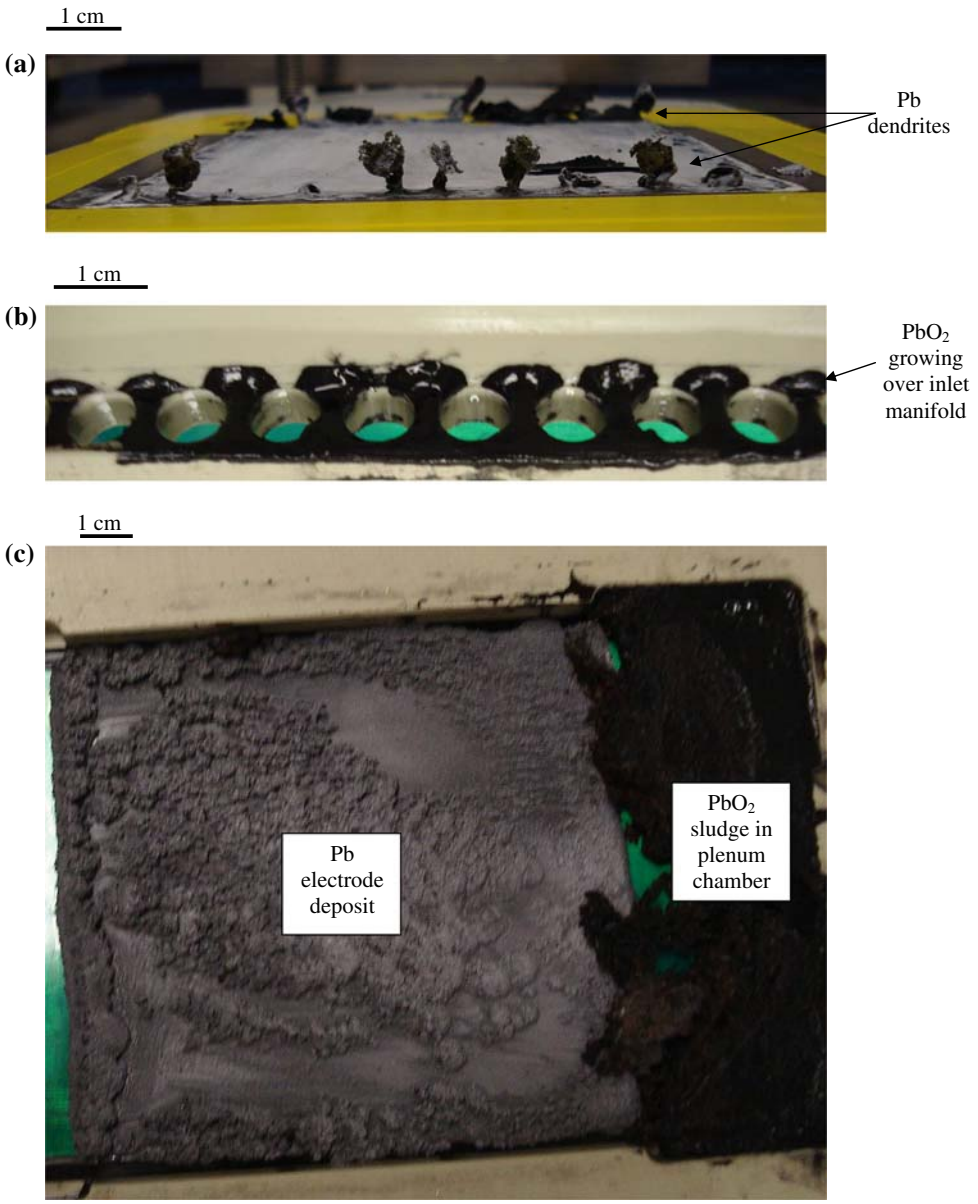

Fig. 10 Photographic images illustrating three failure processes associated with imbalances in the cell chemistry. **a** Pb dendrites. **b** PbO_2 creeping along the cell wall from the positive electrode towards the negative electrode. **c** PbO_2 sludge accumulating on the positive electrode

- Pb dendrite growths can bridge the inter-electrode gap causing an electrical short (Fig. 10a).
- PbO_2 creep over non-conducting surfaces adjacent to the electrodes, such as inlet manifolds or cell spacers (Fig. 10b). These deposits are well-adhered structural PbO_2 growths. Once nucleated, these growths are difficult to remove with simple battery discharging and over time, bridge the inter-electrode gap, causing electrical shorting.
- PbO_2 sludge resulting from loss of PbO_2 particles from the positive electrode (Fig. 10c). These deposits are gel-like accumulations of debris from the positive electrode. They are generally quite soft and particulate in nature. They can either form a film over the positive electrode, reducing charge/discharge efficiencies or sediment in areas of low electrolyte flow, causing an electrical short-circuit between the positive and negative electrode.

4 Conclusions

(a) A scaled-up soluble lead-acid flow battery has been demonstrated, operating both as a single cell and as a bipolar, two-cell stack. Using short charge times (900 s at $\leq$20 mA cm^{-2}) the battery successfully runs for numerous charge/discharge cycles. However, with longer charge times (i.e., thicker Pb and PbO_2 electrode deposits) the cell performance significantly drops off after a few tens of cycles.

(b) Three possible failure processes associated with the cell chemistry have been observed; Pb dendrites, PbO_2 creep, and PbO_2 sludging. All three processes resulted in electrical shorting between the positive and negative electrodes. Dendritic Pb growths typically occurred after high current charging and discharging. PbO_2 creep refers to solid, well-adhered PbO_2 deposits growing over the polymer cell components, eventually bridging the interelectrode gap. PbO_2 sludging refers to amorphous, gel-like deposits forming from debris removed from the positive electrode. These deposits build up in areas of low electrolyte flow and through sedimentation onto horizontal cell components, such as electrode spacers and inlet manifolds.

(c) Failure of the battery due to PbO_2 sludge and PbO_2 creep was more noticeable when using the flow chamber configurations 'B' and 'C'. The plenum chamber acted as a support surface for PbO_2 sedimentation and as a growth support for PbO_2 electrodeposits.

5 Further work

While these preliminary studies have demonstrated operation of the soluble lead-acid flow cell on a large scale, it is recognized that much still needs to be achieved before large-scale applications (e.g., load levelling) could be considered. In particular, it is essential to improve control of the form and adhesion of the deposits on the electrodes to improve further cycle life of the battery, especially with longer charge times up to 6 h when the Pb and PbO_2 deposits will be much thicker. In later papers, the influence of current density during charge and discharge, charge and discharge times, and concentration of both Pb^{2+} and H^+ on cycle life as well as in situ methods for regeneration of both electrodes and electrolyte will be reported. In addition to the use of electrolyte additives to control the deposition and dissolution characteristics, the optimization of the inlet/outlet manifolds and cell-chamber design will be discussed. Operation of the 100 cm^2 C-Tech Innovation Limited flow cell as a bipolar stack is also planned together with further scale-up of the technology to multiple (<10) larger (<1,200 cm^2) electrode areas.

Acknowledgements The authors are grateful for financial support via a DTI Technology Programme Contract TP/4/EET/6/I/2296 entitled '*Redox Flow Cells for Intelligent Grid Management*'. The partners in this project, C-Tech Innovation Limited and E-ON UK, have contributed to the realization of data. In particular, the authors are grateful to Mr. J. Bateman of E-ON UK for valuable discussions. Parts of this paper were presented by F.C. Walsh in a plenary lecture to the 8th European Electrochemical Engineering Symposium, Prague, August 24–28, 2008.

References

1. Frias-Ferrer A, Gonzalez-Garcia J, Szánto DA, Ponce-de-León C, Walsh FC (2006) J Power Sourc 160:716
2. Schrodt JP, Otting WT, Schoegler JO, Craig DN (1946) Trans Electrochem Soc 90:281
3. White JC, Powers WH, McMurtric RL, Pierce RT (1947) Trans Electrochem Soc 91:21
4. White JC, Balwin JH, Peebles EJ, Powers WH (1949) Lead perchloric acid primary cell. United States Patent 2,492,206
5. McDonald GD, Weissman EY, Roemer TS (1972) J Electrochem Soc 119:660
6. Beck F (1977) Lead batteries. United States Patent 4,001,037
7. Wurmb R, Beck F, Boehlke K (1978) Secondary battery. United States Patent 4,092,463
8. Henk P (1982) Lead salt electric storage battery. United States Patent 4,331,744
9. Pletcher D, Hazza A, Wills RGA (2004) Phys Chem Chem Phys 6:1773
10. Pletcher D, Wills RGA (2004) Phys Chem Chem Phys 6:1779
11. Pletcher D, Wills RGA (2005) J Power Sourc 149:96
12. Pletcher D, Hazza A, Wills RGA (2005) J Power Sourc 149:103

13. Pletcher D, Zhou H, Low CTJ, Kear G, Wills RGA, Walsh FC (2008) J Power Sourc 180:621
14. Pletcher D, Zhou H, Low CTJ, Kear G, Wills RGA, Walsh FC (2008) J Power Sourc 180:630
15. Clarke RL, Dougherty BJ, Harrison S, Millington JP, Mohanta S (2006) Battery with bifunctional electrolyte. United States Patent 6,986,966
16. Brown CJ, Hammond JK, Pletcher D, Robinson D, Walsh FC (1992) Mass transport in ICI's filter-press monopolar electrolyser. In: Kreysa G (ed) Part II—laboratory studies in the FM01-LC reactor, Dechema Monograph, vol 123. VCH, Weinheim, pp 299–315
17. Brown CJ, Pletcher D, Walsh FC, Hammond JK, Robinson D (1993) J Appl Electrochem 23:38
18. Griffiths M, Ponce-de-León C, Walsh FC (2005) A.I.Ch.E Journal 51(2):682